In Situ Spectroscopy with Laboratory Nano-XRM

By Jeff Gelb | Sigray, Inc

ABSTRACT | By enabling access to 3 different x-ray energies (the first ever laboratory nanoXRM with "energy tunability" through a patented x-ray illumination beam system), the TriLambda 3D nano x-ray microscope (nano-XRM) provides powerful new capabilities to quantify microstructure and distinguish between materials that would otherwise appear similar in x-ray imaging.

INTRODUCTION

In laboratory absorption-contrast tomography, material differences are observed by changes in grey levels, often called CT numbers. These changes in grey levels are generally formed through attenuation of the X-ray beam, which is termed contrast and follows the Lambert-Beer law, as in Figure 1 below.

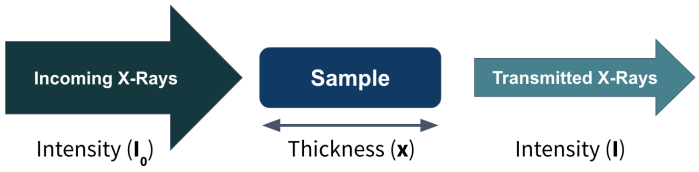

$$Transmission\ (\tau) = \frac{I}{I_0} = e^{-k(E)*x}$$

$$Contrast = \frac{I_0 - I}{I_0 + I} = \frac{1-\tau}{1+\tau}$$

Figure 1: X-ray contrast is a function of material type, feature size, and photon energy.

Attenuation of the X-ray beam is unique to each element, scaled by an energy-dependent parameter k (the mass-attenuation coefficient of the material). Thus, contrast is energy-dependent, and generally follows exponential decay as energy is increased, as shown in Figure 2.

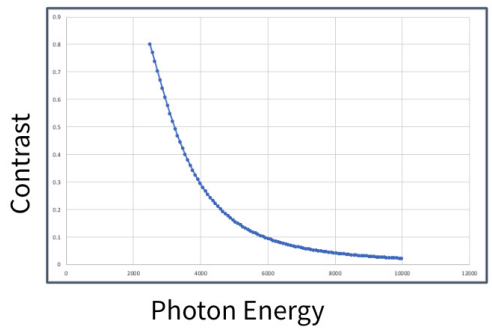

Figure 2: Contrast as a function of photon energy, assuming 10 µm thickness of carbon.

However, the CT numbers may sometimes be misleading. Sub-resolution features, such as nanoporosity or nano-scale alloying elements, may artificially reduce CT numbers to unexpected values, which can lead to errors in image segmentation and, ultimately, inaccurate quantification of the atomic number of the material and its microstructure.

The exponential decay is, by nature, discontinuous. At certain energies, the element exhibits an "absorption edge" at the x-ray energy that matches the exact energy of an electron shell transition, and which is unique to the specific element (Figure 3). This means that elements will produce substantially higher contrast at specific energies with a discontinuous contrast enhancement as compared to neighboring elements. Figure 3 shows a range of transition metals that exhibit higher contrast at, for example, 8.0 keV as compared to 5.4 keV, two of the standard x-ray energies provided by Sigray TriLambda NanoXRM.

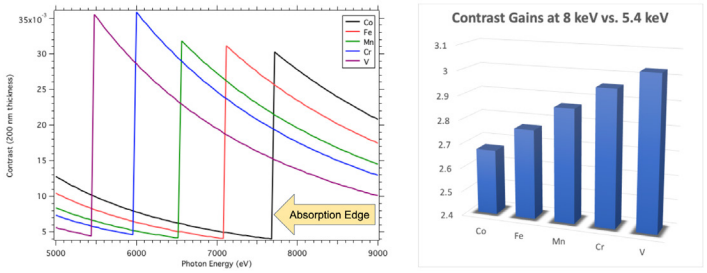

Figure 3: Left: Discontinuous contrast enhancement is expected for transition metals. Right: By using two different x-ray excitation energies (8 keV using a Cu target and 5.4 keV using a Cr target), contrast gains are expected for these transition metals due to the discontinuous edge contrast enhancement.

The discontinuities are used routinely in synchrotron facilities to more precisely identify certain materials of interest, and full-field transmission x-ray microscopy (XRM) featuring absorption-edge spectroscopy (XAS) is now commonly performed at advanced imaging beamlines worldwide. However, implementing this approach in the laboratory has previously been impractical; nearly all commercially available laboratory x-ray sources are single energy or require hours or days to swap between targets (e.g., in some rotating

anodes). Moreover, the system must be reconfigured for each x-ray energy, as all components (condensers, zoneplates, phase rings) are specific to each energy.

Sigray TriLambda Nano-XRM is designed around a patented ultrahigh brightness multi-target x-ray illumination beam system. Each of the three x-ray targets produces a different x-ray spectrum. The TriLambda allows users to rapidly switch between three different energies with little-to-no reconfiguration required. The push-button operation of the energy control now enables imaging at a variety of energies, opening opportunities for in situ spectroscopy while maintaining the high resolution of the nano-XRM. Here, we explore this technique as it is applied to a material system containing known quantities of iron (Fe), one of the commonly-studied elements at synchrotron nano-XRM beamlines.

MATERIALS AND METHODS

Samples used for this initial investigation were specially-prepared Li-ion battery electrodes, containing a graphite particle structure at 95 wt%, 2.5 wt% PVDF binder, and 2.5 wt% carbon-coated iron nanoparticles (Fe NPs). Details on the origin and fabrication of this electrode structure are discussed elsewhere [1]. The sample was trimmed to a small point and mounted to a needle for X-ray imaging, as shown in Figure 4. Prior to performing X-ray microscopy, scanning-electron micrographs were collected to inspect the surface microstructure (Fig. 5), which revealed a spatially-inhomogeneous distribution of Fe NPs, thus indicating a need for 3D imaging of this microstructure.

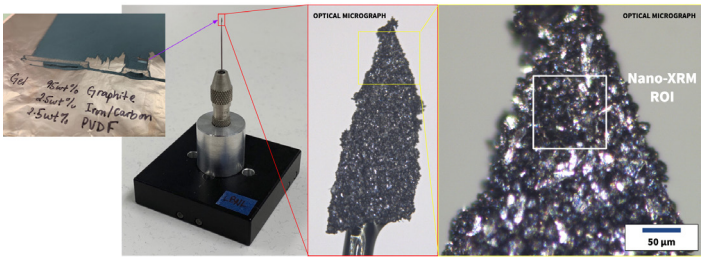

Figure 4: (left to right) Photogaph of the raw material, photo of the specimen as mounted in the sample holder, low resolution optical micrograph of the prepared section, and high-resolution optical micrograph showing the nano-XRM region of interest.

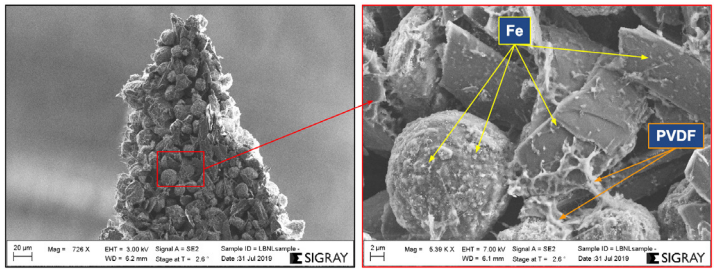

Figure 5: SEM micrographs of the graphite battery anode as prepared for nano-XRM. The Fe NPs are visible in disperse clusters around the active material and throughout the PVDF binder.

Nano-scale X-ray microscopy was performed using Sigray TriLambda Nano-XRM, imaging first with the Cu target and then re-imaging the same ROI with the Cr target, adjusting exposure times for equivalent dose per unit volume between scans. Example projection radiographs of the sample at each energy are shown in Figure 6 below. Each radiograph series was reconstructed using the Gridrec routine in TomoPy [2], then the resulting 3D tomograms were registered to each other and aligned using Avizo 2019.2 (Thermo Fisher Scientific, Hillsborough, OR, USA).

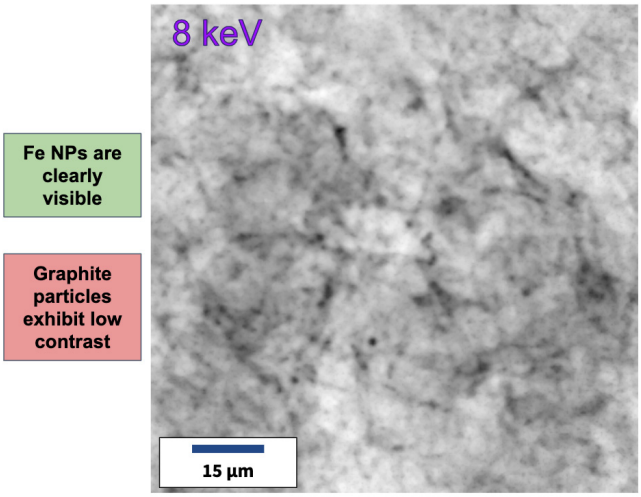

Figure 6: Example radiograph images using the 8 keV Cu target (top) and 5.4 keV Cr target (bottom). At 5.4 keV, higher contrast is observed for the graphite particles, while 8 keV exhibits higher contrast for the iron particles.

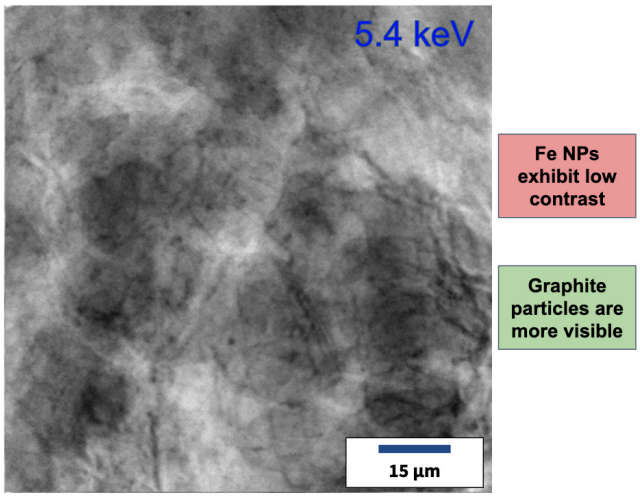

RESULTS AND DISCUSSION

Example virtual slices from each 3D volume are shown in Figure 7. From theory [3], one may expect a ~300% contrast enhancement on the graphite particles at 5.4 keV as compared to 8 keV, shown in Figure 8 below. Thus, the CT numbers in the 5.4 keV dataset were scaled to 30% of their initial values in order to match the graphite CT numbers at 5.4 keV to the graphite CT numbers at 8 keV, which had a negligible effect on the Fe CT numbers at 5.4 keV.

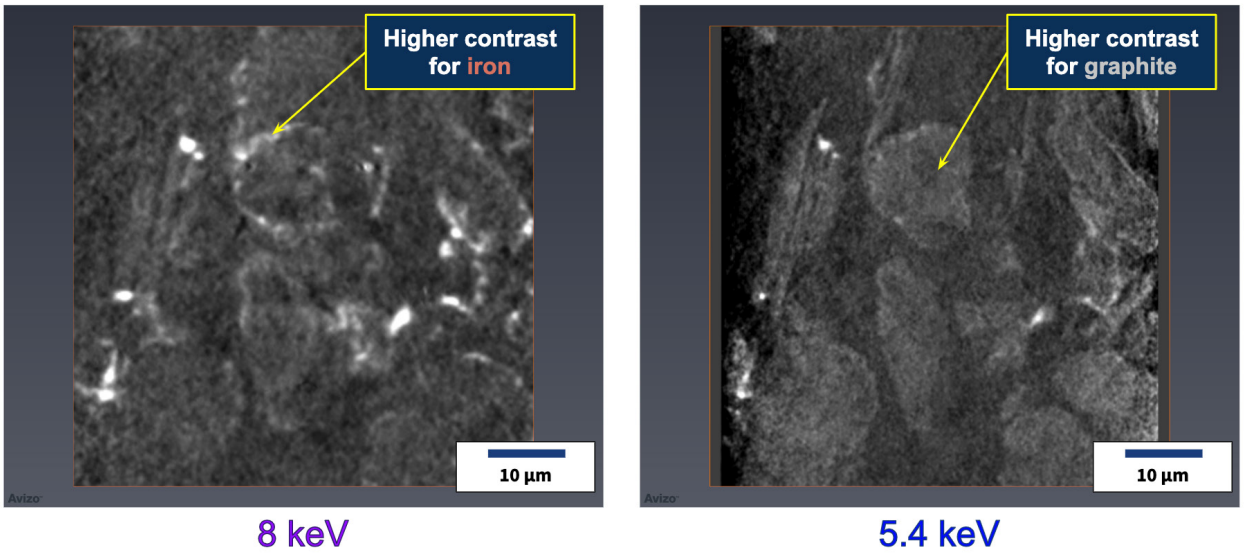

Figure 7: Example virtual slices from each 3D volume, showing the tomographic contrast enhancement of the Fe NPs at 8 keV.

By subtracting the scaled 5.4 keV dataset from the original 8 keV dataset, the graphite particles were expected to cancel out, leaving behind only information on the Fe NPs. Figure 9 shows virtual slices (tomograms) of the composite image formed through weighted subtraction, and Figures 10-11 show the tomograms rendered into 3D volumes with the Fe NPs clearly isolated.

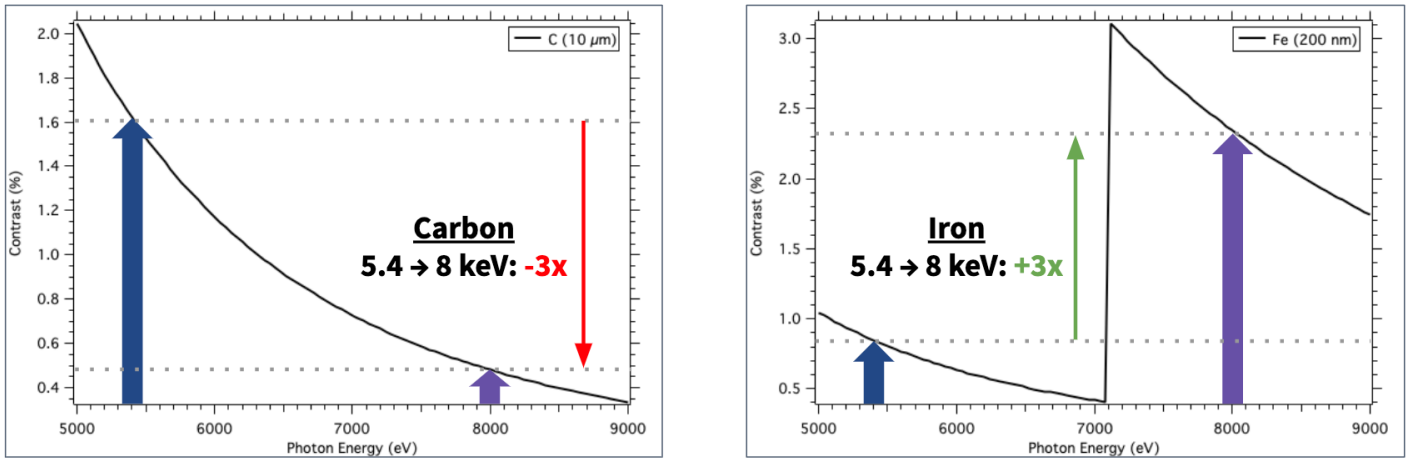

Figure 8: Contrast of graphite at 5.4 keV is expected to be 3x higher than the contrast at 8 keV, while the inverse is true for iron. Scaling the 5.4 keV dataset by 30% and subtracting the result from the 8 keV dataset is expected to cancel the graphite, while retaining the iron signals.

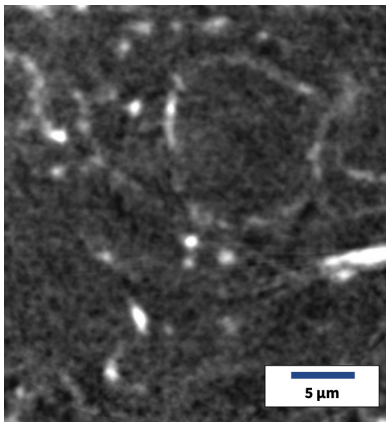

Figure 9: Virtual slice from the 3D difference image. Bright features are isolated Fe NPs (and Fe NP clusters), while all other internal features have been cancelled through the subtraction operation.

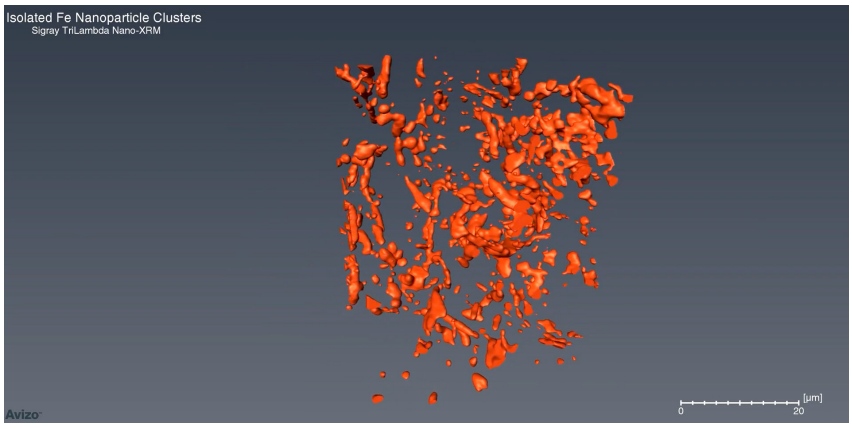

Figure 10: 3D surface rendering of the segmented Fe NPs, isolated with high certainty through the dual-energy nanotomography approach with Sigray TriLambda NanoXRM.

SUMMARY

Interpreting contrast measurements and CT numbers may be a difficult task when only a single X-ray energy is used for imaging. By implementing a dual-energy nanotomography approach, Sigray TriLambda NanoXRM enables quasi-quantitative spectroscopy in situ, providing 3D volumetric contrast enhancement for a range of materials. While now an established technique in synchrotron facilities worldwide, this is the first demonstration of dual-energy nanotomography using a laboratory nano-XRM. The technique introduced here is uniquely possible due to the multi-target configuration of Sigray TriLambda, providing energy tunability as a switchable parameter while retaining the 40 nm spatial resolution capabilities of the instrument.

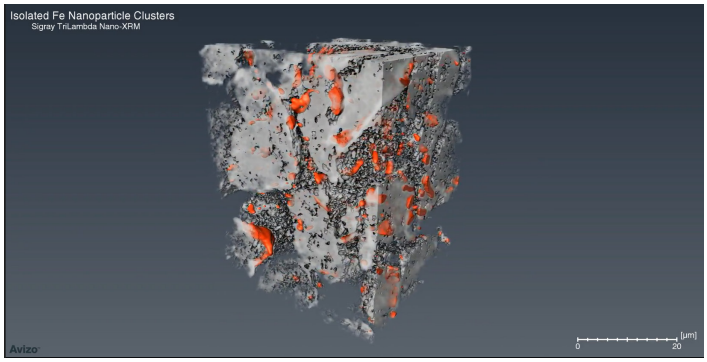

Figure 11: 3D surface rendering of the segmented Fe NPs (orange) in relation to the graphite clusters (grey)

ACKNOWLEDGEMENTS

The authors gratefully acknowledge the help and collaboration of Dr. Stephen J. Harris (Lawrence Berkeley National Laboratory, Berkeley, CA, USA), as well as Prof. Maureen Tang and Dr. Samantha Morelly (Drexel University, Philadelphia, PA, USA) for their work in fabricating the Fe-doped battery electrodes.

References

[1] S. L. Morelly, J. Gelb, F. Iacoviello, P. R. Shearing, S. J. Harris, N. J. Alvarez, and M. H. Tang, "Three-Dimensional Visualization of Conductive Domains in Battery Electrodes with Contrast-Enhancing Nanoparticles," ACS Appl. Energy Mater., vol. 1, no. 9, pp. 4479–4484, Sep. 2018.

[2] D. Gursoy, F. De Carlo, X. Xiao, and C. Jacobsen, "TomoPy: a framework for the analysis of synchrotron tomographic data," J. Synchrotron Rad (2014). 21, 1188-1193 [doi:10.1107/S1600577514013939], pp. 1–6, Aug. 2014.

[3] B. L. Henke, E. M. Gullikson, and J. C. Davis, "X-Ray Interactions: Photoabsorption, Scattering, Transmission, and Reflection at E = 50-30,000 eV, Z = 1-92," Atomic Data and Nuclear Data Tables, vol. 54, no. 2, pp. 181–342, 1993.

SIGRAY

5750 Imhoff Drive, Suite I,
Concord, CA 94520 USA
P: +1-925-446-4183
sigray.com
info@sigray.com